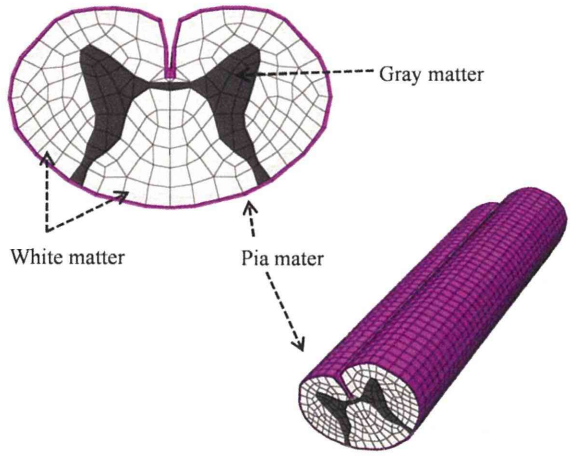

Figure 1 The 3D-FEM model of the spinal cord consists of gray matter, white matter, and pia mater.

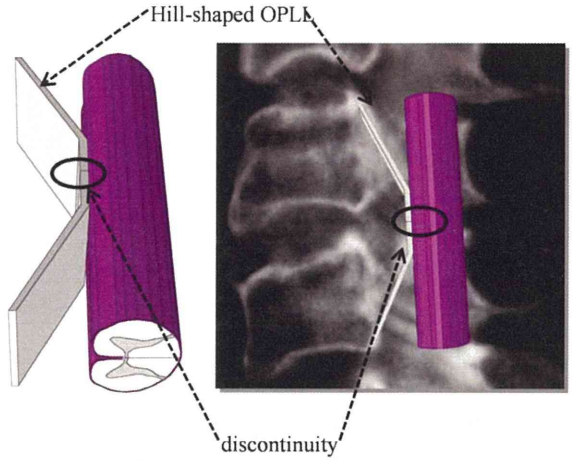

Figure 2 A rigid, hill-shaped body with a slope of 30° was used to simulate C-OPLL. The center of the hill-shaped OPLL established discontinuity. In addition, the upper and lower edges of the hill-shaped OPLL were set to match the posterior upper and lower edges of the vertebral body.

study consisted of gray matter, white matter, and pia mater (Fig. 1). In order to simplify calculation in the model, the denticulate ligament, dura, and nerve root sheaths were not included. The pia mater was included since it has been demonstrated that spinal cord with and without this component shows significantly different mechanical behavior.[8] The spinal cord was assumed to be symmetrical about the mid-sagittal plane, such that only half the spinal cord required reconstruction and the whole model could be integrated by mirror image. The vertical length of spinal cord for CTM measurement was two vertebral bodies (about 40 mm).

Iwasaki *et al.* reported that neurological outcomes following laminoplasty for C-OPLL were only poor or fair in patients with an occupying ratio >60% and/or hill-shaped ossification.[9] The rigid, hill-shaped body with a slope of 30° was used to simulate C-OPLL by measuring paper (Fig. 2).[9] To assume a segmental range of motion (ROM) at the level of maximum cord compression, the center of hill-shaped OPLL was established discontinuity. In addition, upper and lower edges of the hill-shaped OPLL were matched to the posterior upper and lower edges of the vertebral body (Fig. 2).

The lamina model was established by measuring CTM, magnetic resonance imaging, and simulated C-OPLL (Fig. 3).

The spinal cord consists of three distinct materials referred to as white matter, gray matter, and pia mater. The mechanical properties (Young's modulus and Poisson's ratio) of the gray and white matter were determined using data obtained by the tensile stress–strain curve and stress relaxation under various strain rates.[10,11] The mechanical properties of pia mater were obtained from the literature.[12] The mechanical properties of hill-shaped ossification and lamina were stiff enough for the spinal cord to be pressed. Based on the assumption that no slippage occurs at the interfaces of white matter, gray matter, and pia mater, these interfaces were glued together. Since there are no data on the friction coefficient between lamina and spinal cord, this was assumed to be frictionless. Similarly, the coefficient of friction between the hill-shaped ossification and spinal cord was assumed to be frictionless at the contact interfaces.

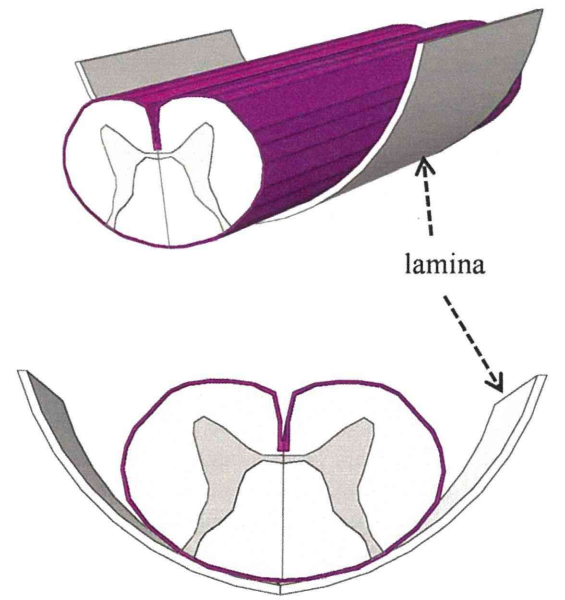

Figure 3 The lamina model was established at the rear of the spinal cord.

The spinal cord, hill-shaped ossification, and lamina model were symmetrically meshed with 15- or 20-node elements. The total number of elements was 11 438 and the total number of nodes was 67 434.

For the static compression model, compression was simulated by C-OPLL with a hill-shaped ossification. The top and bottom of the spinal cord and the lamina were fixed in all directions and then anterior static compression at 10, 20, and 30% of the anterior–posterior (AP) diameter of the spinal cord was applied by the OPLL (Fig. 4A).

For the dynamic compression model, the top and bottom of the spinal cord as well as the lamina were fixed. The lower and upper edges of the OPLL were rotated 2.5° (total 5°), 5° (total 10°), and 7.5° (total 15°) to the flexion direction as a segmental ROM to match the movement of the vertebral body without anterior static compression by OPLL (Fig. 4B).

For the combined static (10%) and dynamic compression model under fixed of for the top and bottom of the spinal cord and lamina, static compression to the spinal cord of 10% of the AP diameter of the spinal cord was applied by OPLL. In this state of compression, the lower and upper edges were rotated 2.5° (total 5°), 5° (total 10°), and 7.5° (total 15°) to the flexion direction as ROM (Fig. 4C).

For the combined static (20%) and dynamic compression model under fixed of for the top and bottom of the spinal cord and lamina, static compression to the spinal cord of 20% of the AP diameter of the spinal cord was applied by OPLL. In this state of compression, the lower and upper edges were rotated 2.5° (total 5°), 5° (total 10°), and 7.5° (total 15°) to the flexion direction as ROM (Fig. 4C).

In total, 12 different compression combinations were evaluated and the average *von Mises* stress was recorded for each cross section.

Results

In the static compression model, stresses were very low under the condition of 10% compression of the AP diameter of the spinal cord. At 20% compression, the stress distributions were confined to gray matter and the anterior funiculus. At 30% compression, the stresses

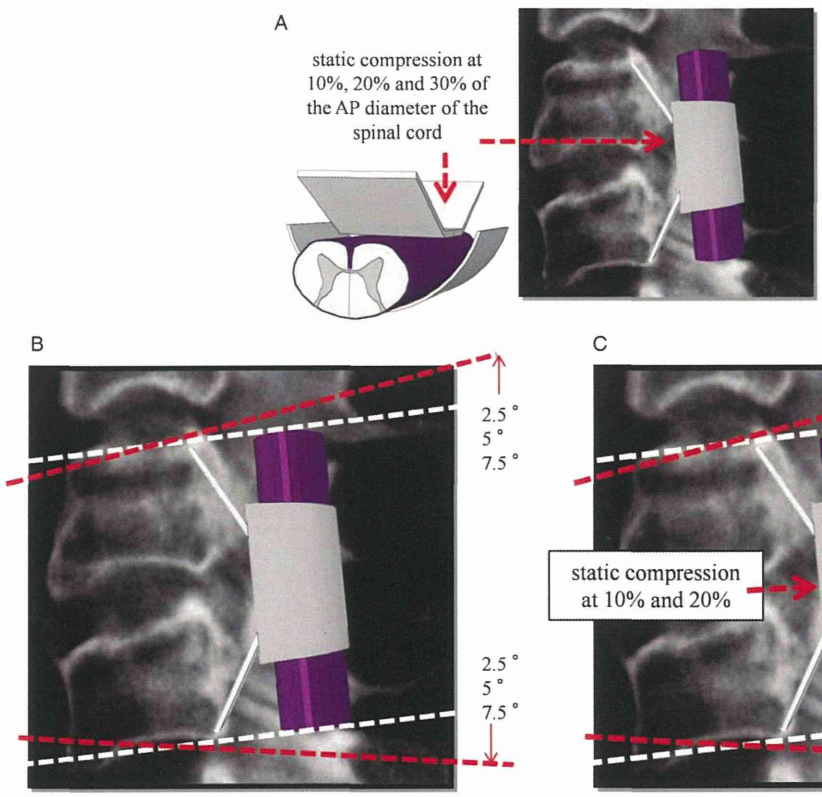

Figure 4 For the static model, anterior static compression at 10, 20, and 30% of the AP diameter of the spinal cord was applied to the spinal cord by the OPLL (A). For the dynamic compression model, the lower and upper edges of OPLL were rotated at 2.5° (total 5°), 5° (total 10°), and 7.5° (total 15°) to the flexion direction as the ROM (B). For the combined static and dynamic model, anterior static compression was 10 and 20% of the AP diameter of the spinal cord and the lower and upper edges of OPLL were rotated at 2.5° (total 5°), 5° (total 10°), and 7.5° (total 15°) to the flexion direction as the ROM (C, D).

ONLINE COLOUR ONLY

on gray matter, anterior funiculus, lateral funiculus, and posterior funiculus were all increased (Fig. 5A).

For the dynamic compression model with 5° ROM, stresses on the spinal cord were very low. A 5° ROM corresponds to ~9% compression of the AP diameter of the spinal cord at the maximal compression site. At 10° ROM, stress distributions were confined to the gray matter and the anterior funiculus. A 10° ROM corresponds to about 16% compression of the AP diameter of the spinal cord at the maximal compression site. The stresses increased at 15° ROM, which corresponds to about 25% compression of the AP diameter of the spinal cord at the maximal compression site (Fig. 5B).

For the combined static (10%) and dynamic compression model, at 5° ROM, the stress distributions were higher than for 10% static compression alone, but were still quite low. This corresponded to about 19% compression of the AP diameter of the spinal cord at the maximal compression site. At 10° ROM, stress appeared in the gray matter and anterior funiculus, while at 15° ROM the stresses on gray matter, anterior funiculus, lateral funiculus, and posterior funiculus all increased. A 10° ROM corresponds to ~26% compression of the AP diameter of the spinal cord at the maximal compression site while a 15° ROM corresponds to about 35% compression (Fig. 5C).

For the combined static (20%) and dynamic compression model, at 5° ROM, the stress distributions were higher than for 20% static compression alone. At 10° ROM, stresses appeared in the spinal cord and increased further at 15° ROM (Fig. 5D). A 5° ROM corresponds to about 29% compression of the AP diameter of the spinal cord at the maximal compression site, 10° ROM corresponds to about 36% compression, and 15° ROM corresponds to about 45% compression.

Discussion

The development of myelopathy significantly affects the prognosis of patients with OPLL in the cervical spine.

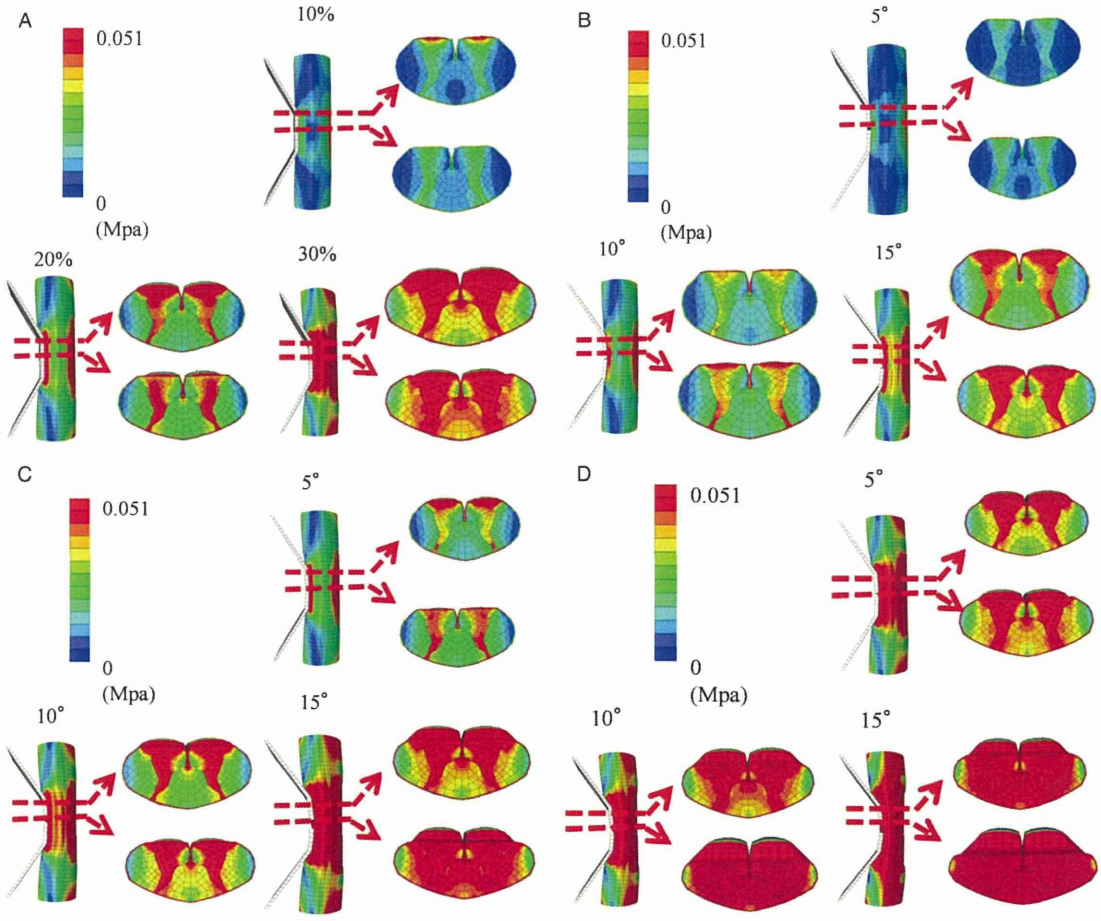

Figure 5 Stress distributions in proximal and central area of compression by C-OPLL are shown for the static compression model (A), the dynamic compression model (B), the combined static (10%) and dynamic compression model (C), and the combined static (20%) and dynamic compression model (D).

ONLINE COLOUR ONLY

Matsunaga *et al.*[1] reported that when the space available for the spinal cord (SAC, static compression factor) was <6 mm, this could induce myelopathy of the cervical spine. Koyanagi *et al.*[13] reported that the proportion of patients showing motor deficits of the lower extremities increased significantly when the sagittal canal diameter of CT was narrowed to <8 mm. Matsunaga *et al.*[7] further reported that all patients with >60% spinal canal stenosis due to OPLL exhibited myelopathy. These findings indicate that static compression is an important factor in myelopathy associated with C-OPLL and that pathologic compression beyond a certain critical point may indeed be the most significant causal factor. Prior to these studies, it was believed that dynamic factors were largely responsible for the development of myelopathy associated with C-OPLL. Matsunaga *et al.*[1] found that ROM of the cervical spine was significantly greater in patients with myelopathy and whose SAC diameter was >6 mm. Azuma *et al.* concluded that C-OPLL myelopathy was induced by static factors, dynamic factors, or a combination of both. To evaluate the contribution of each factor and the responsible level, they measured SAC and ROM at each vertebral and intervertebral level and determined the responsible level by spinal cord-evoked potentials.[6] Fujiyoshi *et al.*[5] reported that patients with massive OPLL did not develop myelopathy and the mobility of their cervical spine was highly restricted. These workers concluded that dynamic factors such as segmental ROM preferentially contributed to the development of myelopathy in patients with C-OPLL.

Using this prior knowledge, we investigated whether static factors and segmental ROM of the responsible level (dynamic factor) in C-OPLL were associated with stresses in the spinal cord. Our first goal was to develop a 3D-FEM spinal cord model that simulates the clinical situation, while our second goal was to analyze the clinical condition of patients. Similar to previous studies by Kato *et al.*,[14–16] Li and Dai,[17,18] and Nishida *et al.*,[19–21] bovine spinal cord was used in the current analytical model since it was impossible to obtain fresh human spinal cord. The mechanical properties of the spinal cord used in our study were similar to earlier reports.[15–21] Xin-Feng *et al.* noted that it was reasonable to use the mechanical properties of bovine spinal cord because the brain and spinal cord of cattle and humans show similar injury-induced changes.[17] For the purpose of this study, we therefore assumed that the mechanical properties of spinal cord from these two species were similar. Cecilia *et al.*[8] reported on the division of spinal cord into pia mater and white and gray matter. These workers showed that the presence of pia mater had a significant effect on spinal cord deformation. Pia mater was therefore included in our model in order to accurately simulate the clinical situation.

Our study was limited to the investigation of stress distribution caused by compression. The amount of compression of the spinal cord does not appear to correlate directly with myelopathy. Furthermore, morphological evidence of apoptosis and molecular changes in the gray and white matter did not correlate with the amount and time of compression. There is currently a dearth of information in the literature on the relationship between myelopathy and the amount and time of compression. Other causal factors that could contribute to C-OPLL include ischemia, congestion, and spinal cord stretch injury.[22] Blood flow and a possible influence of the ligamentum flavum via neck extension were not factored into our FEM analysis and only one movement (neck flexion) was investigated as dynamic factor in C-OPLL. Discontinuity of OPLL was set in the center of OPLL. Long-term compression and apoptotic factors were not considered in the FEM analysis. Moreover, the FEM model used here was simplified in order to facilitate the calculations. Analysis errors were reduced by using a FEM mesh, by assuming the spinal cord was symmetric, by not including the denticulate ligament, dura, and nerve root sheaths, and by setting a close distance between the spinal cord and lamina and between the spinal cord and OPLL. The results for stress distributions may vary if the denticulate ligament is included, since traction is also applied to the spinal cord. Furthermore, because compression is applied in the OPLL model, results may differ in the presence of osteophytes. The ligamentum flavum has a pincer-like movement mechanism that could also influence the results. However, to date there are no published papers on the relationships between osteophytes, ligamentum flavum, and discontinuity of OPLL on the compression of the spinal cord.

In pathology-based studies, Ono *et al.*[23] and Ogino *et al.*[24] described how patients with severe myelopathy showed spinal cord atrophy and presented with extensive degeneration and infarction of the entire gray matter and white columns, except for the anterior funiculus. In the present analysis, stress distributions in the anterior funiculus also increased. However, this increase was not associated with clinical symptoms or with apoptosis; hence, the current results merely provide an estimate for the possible range of increased stress distribution at this site. Nevertheless, the observed stress distribution of OPLL under dynamic motion was similar to a prior clinical report and therefore our

results may be applicable to the clinical situation. More complex materials and structural characteristics of the spinal cord model should be included in future investigations.

In the present study, the stress distribution in the spinal cord increased following static compression and dynamic compression by C-OPLL with hill-shaped ossification. However, the stress distribution did not increase throughout the entire spinal cord. Under combined static and dynamic compression, the stress distribution increased in the entire spinal cord at a ROM of $>10°$ even at a static compression of 10% of the AP diameter of the spinal cord. Stress increased in the entire spinal cord under static compression of 20% and dynamic compression at a ROM of $>5°$. As static compression increases, the stress distribution increases, even with a mild ROM. Thus, when both static compression and dynamic compression such as segmental ROM occur, damage to the spinal cord and the progression of symptoms are likely to arise.

Conclusion

We conducted stress analyses in a static compression model, dynamic compression model, and combination static and dynamic compression model of C-OPLL with hill-shaped ossification.

It is possible that symptoms occur under static compression only or under dynamic compression only. However, under static compression, the stress distribution increases with the ROM at the responsible level and this makes it very likely that symptoms will worsen. We conclude that C-OPLL myelopathy is induced by static factors, dynamic factors, and a combination of both. When ROM is large, careful attention must be paid in case the symptoms worsen, even if static compression is small.

Disclaimer statements

Contributors

T.K., Y.K., S.K., and T.T. played role of guidance and modification of research. Y.Y. and Y.I. is cooperator in research.

Funding

None.

Conflicts of interest

None.

Ethics approval

This report does not need ethical approval.

References

1 Matsunaga S, Kukita M, Hayashi K, Shinkura R, Koriyama C, Sakou T, *et al.* Pathogenesis of myelopathy in patients with ossification of the posterior longitudinal ligament. J Neurosurg 2002; 96(2 Suppl):168–72.
2 Matsunaga S, Sakou T, Hayashi K, Ishidou Y, Hirotsu M, Komiya S. Trauma-induced myelopathy in patients with ossification of the posterior longitudinal ligament. J Neurosurg 2002;97(2 Suppl): 172–5.
3 Masaki Y, Yamazaki M, Okawa A, Aramomi M, Hashimoto M, Koda M, *et al.* An analysis of factors causing poor surgical outcome in patients with cervical myelopathy due to ossification of the posterior longitudinal ligament: anterior decompression with spinal fusion versus laminoplasty. J Spinal Disord Tech 2007;20(1):7–13.
4 Morio Y, Nagashima H, Teshima R, Nawata K. Radiological pathogenesis of cervical myelopathy in 60 consecutive patients with cervical ossification of the posterior longitudinal ligament. Spinal Cord 1999;37(12):853–7.
5 Fujiyoshi T, Yamazaki M, Okawa A, Kawabe J, Hayashi K, Endo T, *et al.* Static versus dynamic factors for the development of myelopathy in patients with cervical ossification of the posterior longitudinal ligament. J Clin Neurosci 2010;17(3): 320–4.
6 Azuma Y, Kato Y, Taguchi T. Etiology of cervical myelopathy induced by ossification of the posterior longitudinal ligament: determining the responsible level of OPLL myelopathy by correlating static compression and dynamic factors. J Spinal Disord Tech 2010;23(3):166–9.
7 Matsunaga S, Nakamura K, Seichi A, Yokoyama T, Toh S, Ichimura S, *et al.* Radiographic predictors for the development of myelopathy in patients with ossification of the posterior longitudinal ligament: a multicenter cohort study. Spine 2008;33(24): 2648–50.
8 Cecilia P, Jon S, Richard M. The importance of fluid-structure interaction in spinal trauma models. J Neurotrauma 2011;28(1): 113–25.
9 Iwasaki M, Okuda S, Miyauchi A, Sakaura H, Mukai Y, Yonenobu K, *et al.* Surgical strategy for cervical myelopathy due to ossification of the posterior longitudinal ligament. Part 1: clinical results and limitations of laminoplasty. Spine 2007;32(6): 647–53.
10 Ichihara K, Taguchi T, Yoshinori S, Ituo S, Shunichi K, Shinya K. Gray matter of the bovine cervical spinal cord is mechanically more rigid and fragile than the white matter. J Neurotrauma 2001;18(3):361–7.
11 Ichihara K, Taguchi T, Sakuramoto I, Kawano S, Kawai S. Mechanism of the spinal cord injury and the cervical spondylotic myelopathy: new approach based on the mechanical features of the spinal cord white and gray matter. J Neurosurg 2003;99(3 Suppl):278–85.
12 Tunturi AR. Elasticity of the spinal cord, pia and denticulate ligament in the dog. J Neurosurg 1978;48(6):975–9.
13 Koyanagi I, Imamura H, Fujimoto S, Hida K, Iwasaki Y, Houkin K. Spinal canal size in ossification of the posterior longitudinal ligament of the cervical spine. Surg Neurol 2004;62(4): 286–91.
14 Kato Y, Kanchiku T, Imajo Y, Kimura K, Ichihara K, Kawano S, *et al.* Biomechanical study of the effect of the degree of static compression of the spinal cord in ossification of the posterior longitudinal ligament. J Neurosurg Spine 2010;12:301–5.
15 Kato Y, Kataoka H, Ichihara K, Imajo Y, Kojima T, Kawano S, *et al.* Biomechanical study of cervical flexion myelopathy using a three-dimensional finite element method. J Neurosurg Spine 2008;8(5):436–41.
16 Kato Y, Kanchiku T, Imajo Y, Ichinara K, Kawano S, Hamanama D, *et al.* Flexion model simulating spinal cord injury without radiographic abnormality in patients with ossification of the longitudinal ligament: the influence of flexion speed on the cervical spine. J Spinal Cord Med 2009;32(5):555–9.
17 Li XF, Dai LY. Three-dimensional finite element model of the cervical spinal cord. Spine (Phila Pa 1976) 2009;34(11):1140–7.
18 Li XF, Dai LY. Acute central cord syndrome: injury mechanisms and stress features. Spine (Phila Pa 1976) 2010;35(19):E955–64.

19 Nishida N, Kato Y, Imajo Y, Kawano S, Taguchi T. Biomechanical study of the spinal cord in thoracic ossification of the posterior longitudinal ligament. J Spinal Cord Med 2011;34(5):518–22.
20 Nishida N, Kato Y, Imajo Y, Kawano S, Taguchi T. Biomechanical analysis of cervical spondylotic myelopathy: the influence of dynamic factors and morphometry of the spinal cord. J Spinal Cord Med 2012;35(4):256–61.
21 Nishida N, Kanchiku T, Kato Y, Imajo Y, Kawano S, Taguchi T. Biomechanical analysis of the spinal cord in Brown–Séquard syndrome. Exp Ther Med 2013;6(5):1184–8.
22 Henderson FC, Geddes JF, Vaccaro AR, Woodard E, Berry KJ. Stretch-associated injury in cervical spondylotic myelopathy: new concept and review. Neurosurgery 2005;56(5):1101–13.
23 Ono K, Ota H, Tada K, Yamamoto T. Cervical myelopathy secondary to multiple spondylotic protrusions. A clinicopathologic study. Spine (Phila Pa 1976) 1977;2(2):109–25.
24 Ogino H, Tada K, Okada K, Yonenobu K, Yamamoto T, Ono K, *et al.* Canal diameter, anteroposterior compression ration, and spondylotic myelopathy of the cervical spine. Spine (Phila Pa 1976) 1983;8(1):1–15.

Authors Queries

Journal: **The Journal of Spinal Cord Medicine**
Paper: **JSCM-D-13-00137**
Article title: **Cervical ossification of the posterior longitudinal ligament: Biomechanical analysis of the influence of static and dynamic factors**

Dear Author
During the preparation of your manuscript for publication, the questions listed below have arisen.
Please attend to these matters and return this form with your proof. Many thanks for your assistance

Query Reference	Query	Remarks
1	Please check and confirm the expansion of AP as 'anterior–posterior' in the abstract as given in the text.	
2	Please provide the supplier name for 'ABAQUS 6.11 (Valley Street, Providence, RI, USA)'.	
3	Please expand CTM.	
4	Please clarify the phrase '...under fixed of for...' as it is not clear in the sentence 'For the combined static...' and elsewhere in the text.	
5	We are having subcaption for Fig. 4d, but figure missing. Please check.	
6	Please expand CT.	
7	Xin-Feng et al. is not matching with reference [17] in the reference list. Please check and confirm.	

ASIAN SPINE JOURNAL
Clinical Study
Asian Spine J 2015;9(4):541-547 • http://dx.doi.org/10.4184/asj.2015.9.4.541

Normal Values of Diffusion Tensor Magnetic Resonance Imaging Parameters in the Cervical Spinal Cord

Kazuki Chagawa[1], Shunka Nishijima[2], Tsukasa Kanchiku[1], Yasuaki Imajo[1], Hidenori Suzuki[1], Yuichiro Yoshida[1], Toshihiko Taguchi[1]

[1]*Department of Orthopedic Surgery, Yamaguchi University Graduate School of Medicine, Ube, Japan*
[2]*Department of Orthopedic Surgery, Sento Hill Hospital, Ube, Japan*

Study Design: Prospective study.

Purpose: We evaluated the usefulness of diffusion tensor imaging (DTI) in diagnosing patients with cervical myelopathy by determining the accuracy of normal DTI parameter values.

Overview of Literature: DTI can visualize white matter tracts *in vivo* and quantify anisotropy. DTI is known to be more sensitive than conventional magnetic resonance imaging (MRI) in detecting subtle pathological changes of the spinal cord.

Methods: A total of 31 normal subjects (13 men and 18 women; age, 23–87 years; mean age, 46.0 years) were included in this study. The patients had no symptoms of myelopathy or radiculopathy. A Philips Achieva 3-Tesla MRI with SE-type Single Shot EPI was used to obtain diffusion tensor images. Apparent diffusion coefficient (ADC) and fractional anisotropy (FA) values were measured as DTI parameters on axial sections of several cervical levels. Subjects were divided into two groups: >40 years (n=16) and ≤40 years (n=15). A paired t-test was used to compare significant differences between the groups. ADC and FA values were most stable on axial sections.

Results: For all subjects, mean ADC and FA values were $1.06\pm0.09\times10^{-3}$ mm^2/sec and 0.68±0.05, respectively. ADC was significantly higher in subjects >40 years of age than in those ≤40 years. There was no significant difference in FA values between the two groups. The mean ADC value was significantly higher in normal subjects >40 years of age than in those ≤40 years.

Conclusions: It is important to consider age when evaluating cervical myelopathy by DTI.

Keywords: Diffusion tensor imaging; Reference values; Cervical spinal cord

Introduction

Diffusion tensor imaging (DTI) is a relatively new magnetic resonance imaging (MRI) technique capable of depicting structural details of the brain and spinal cord white matter. It can assist visualization of white matter tracts *in vivo* and quantify anisotropy [1]. DTI is computed by tensor analysis, which is a multilinear vector parameter that enables determination of the restricted anisotropic diffusion of water molecules in the structures of living organisms such as white matter nerve fibers [2].

DTI results are quantified by two primary parameters:

Received May 25, 2015; Revised May 27, 2015; Accepted May 27, 2015
Corresponding author: Kazuki Chagawa
Department of Orthopedic Surgery, Yamaguchi University Graduate School of Medicine,
1-1-1 Minami-kogushi, Ube 755-8505, Japan
Tel: +81-836-22-2268, Fax: +81-836-22-2267, E-mail: chagawa@yamaguchi-u.ac.jp

Asian Spine Journal • pISSN 1976-1902 eISSN 1976-7846 • www.asianspinejournal.org

the apparent diffusion coefficient (ADC) value, which refers to the overall diffusivity of the tissue irrespective of directional dependence, and the fractional anisotropy (FA) value, which reflects the directional dependence of the diffusion process and is expressed as a relative number ranging from 0 to 1 that increases in relation to the anisotropic diffusion within the tissue being evaluated.

Mamata et al. [3] reported that in nerve fiber impairment, the medullary sheath is destroyed and water molecules exhibit increased diffusion in the direction in which they are normally restricted (i.e., diffusion anisotropy is lost); thus, ADC increases and FA decreases. The spinal cord white matter consists of nerve fiber bundles aligned regularly from head to tail. Water molecules diffuse along the component axons resulting in high anisotropic diffusion within the spinal cord white matter, thus facilitating the usefulness of DTI in spinal cord evaluation.

Some reports have suggested the usefulness of DTI parameters for examining the cervical spinal cord [1,4,5], but little has been reported on normal values of these parameters. For standard implementation of DTI as a examination method for the cervical spinal cord, it is important to study these normal values in more detail.

The aim of this study was to investigate the accuracy of normal values of DTI parameters and determine their usefulness for definitive diagnoses in patients with cervical myelopathy. We also determined if DTI could be used to objectively evaluate function in compressive cervical disease. As a first step, we calculated normal values of DTI parameters in healthy subjects.

Materials and Methods

This study was approved by the Institutional Review Board of Yamaguchi University Hospital and adhered to the tenets of the Declaration of Helsinki.

1. Subjects

A total of 31 healthy adults (13 men, 18 women; age, 23–87 years; mean age, 46.0±18.8 years) participated in this study. Informed consent was obtained prior to the MRI procedure. Ethics approval was obtained from the local Human Research Ethics Board. All subjects who submitted written informed consent met the exclusion criteria for MRI and exhibited no symptoms of myelopathy or radiculopathy. Subjects were divided into two groups on the basis of age—those >40 years old (n=16) and those ≤40 years old (n=15)—and sex (men, n=13; women, n=18). The paired *t*-test was used to identify significant differences between groups. Statistical significance was established at $p<0.05$.

2. Imaging procedures

A 3-T MR scanner (Philips Achieva, Philips Medical System, Eindhoven, The Netherlands) equipped with a 16-channel neurovascular coil was used to perform all examinations from 2010 to 2013. The protocol included conventional sequences to evaluate the spine and spinal cord morphology including T1 and T2. DTI data were acquired by using SE-type Single-Shot EPI sequences. The following scanning parameters were used: TE, 69 ms; TR, 9,079 ms; number of slices, 30; interslice gap, 0 mm; band width, 1,711.8 Hz/pixel; voxel size, 1.79×1.42×4.00 mm; acquisition matrix, 112×140; and number of excitation, 4. Images were acquired with b values of 0 and 700 s/mm^2. The DTI parameters, ADC and FA, were measured on axial sections of several cervical levels (C1/2–C6/7).

As shown in Fig. 1, both ADC and FA images were taken, and intraspinal ADC and FA values were measured between each vertebra from the C1/2 to C6/7 level using an axial image that gave stable values. Because DTI is incapable of capturing an image of multiple stacks simultaneously, individual slices were generated at the C4/5 level (a preferred site) as a reference (Fig. 1A). The region of interest was identified manually in the spinal axial view but did not involve the spinal edge to achieve stable values (Fig. 1B–E).

Results

ADC and FA values were most stable on axial sections. Fig. 2 showed the trends of ADC and FA values, respectively, in the 31 healthy subjects. The average ADC value was 1.06±0.09×10^{-3} mm^2/sec, and the average FA value was 0.68±0.05.

The trend of average ADC values and their standard deviations in the healthy subjects were shown in Fig. 3A. In general, stable values were obtained, but they tended to increase towards the lower cervical levels. As shown in Fig. 3B, a generally stable average FA value was obtained.

Next, we compared normal ADC and FA values according to age. ADC values were significantly higher

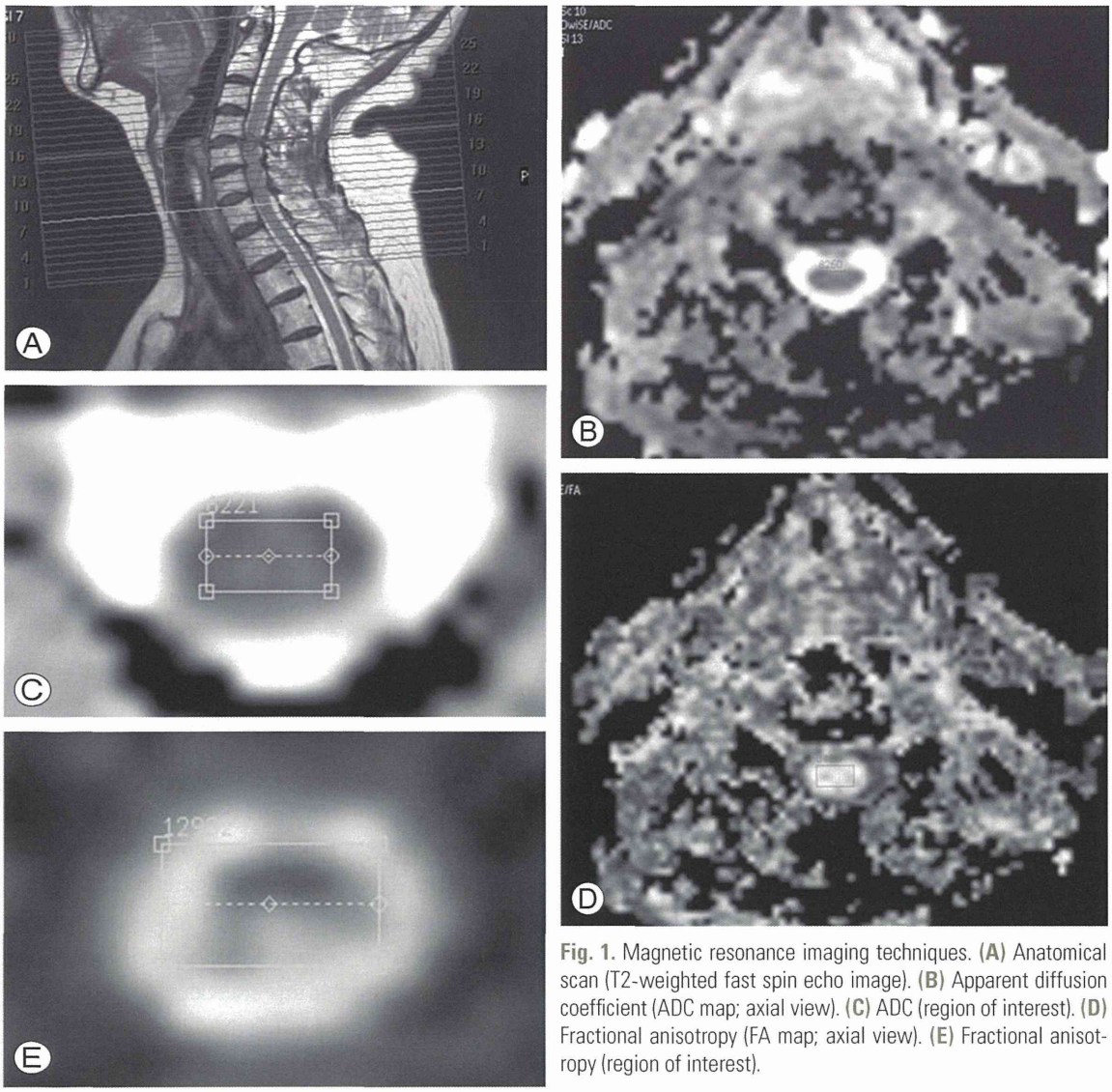

Fig. 1. Magnetic resonance imaging techniques. **(A)** Anatomical scan (T2-weighted fast spin echo image). **(B)** Apparent diffusion coefficient (ADC map; axial view). **(C)** ADC (region of interest). **(D)** Fractional anisotropy (FA map; axial view). **(E)** Fractional anisotropy (region of interest).

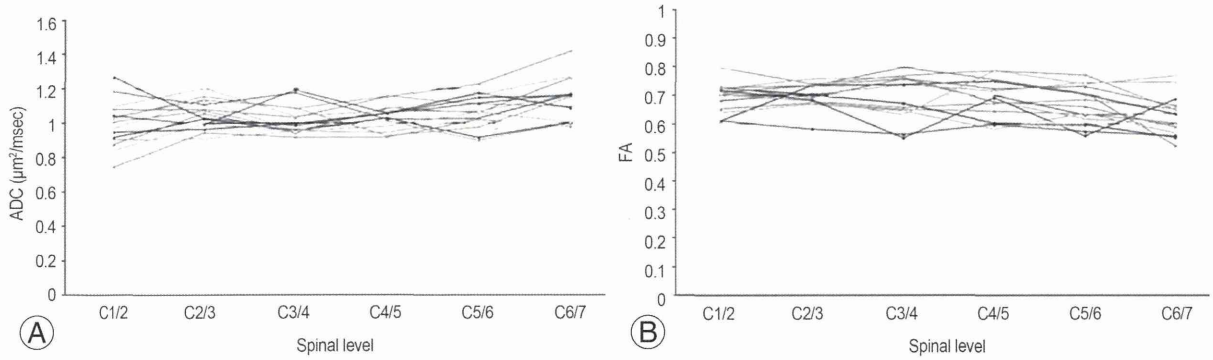

Fig. 2. **(A)** Apparent diffusion coefficient (ADC) in 31 healthy adults; mean ADC=1.06±0.09×10–3 mm^2/sec. **(B)** Fractional anisotropy (FA) in 31 healthy adults; mean FA=0.68±0.05.

in the subjects >40 years of age than in those ≤40 years (p=0.04) (Fig. 4A). Spearman rank correlation coefficient test showed that ADC was positively correlated with age (p=0.02) (Fig. 4B).